HHS Public Access

Author manuscript

Cell. Author manuscript; available in PMC 2016 December 17.

Published in final edited form as:

Cell. 2015 December 17; 163(7): 1770–1782. doi:10.1016/j.cell.2015.11.022.

Control of synaptic connectivity by a network of *Drosophila* IgSF cell surface proteins

Robert A. Carrillo[#1], **Engin Özkan**[#2,4,¶], **Kaushiki P. Menon**[#1], **Sonal Nagarkar-Jaiswal**[3], **Pei-Tseng Lee**[3], **Mili Jeon**[1,4], **Michael E. Birnbaum**[4], **Hugo J. Bellen**[3], **K. Christopher Garcia**[4], and **Kai Zinn**[1,¶]

[1]Division of Biology and Biological Engineering, California Institute of Technology, Pasadena, CA

[2]Dept. of Biochemistry and Molecular Biology, University of Chicago, Chicago, IL

[3]Howard Hughes Medical Institute, Program in Developmental Biology, Dept. of Molecular and Human Genetics, Jan and Dan Duncan Neurological Research Institute at TCH, Baylor College of Medicine, Houston, TX

[4]Howard Hughes Medical Institute, Depts. of Molecular and Cellular Physiology and Structural Biology, Stanford University School of Medicine, Stanford, CA

[#] These authors contributed equally to this work.

Summary

We have defined a network of interacting *Drosophila* cell surface proteins in which a 21-member IgSF subfamily, the Dprs, binds to a 9-member subfamily, the DIPs. The structural basis of the Dpr-DIP interaction code appears to be dictated by shape complementarity within the Dpr-DIP binding interface. Each of the 6 *dpr* and *DIP* genes examined here is expressed by a unique subset of larval and pupal neurons. In the neuromuscular system, interactions between Dpr11 and DIP-γ affect presynaptic terminal development, trophic factor responses, and neurotransmission. In the visual system, *dpr11* is selectively expressed by R7 photoreceptors that use Rh4 opsin (yR7s). Their primary synaptic targets, Dm8 amacrine neurons, express *DIP-γ*. In *dpr11* or *DIP-γ* mutants, yR7 terminals extend beyond their normal termination zones in layer M6 of the medulla. DIP-γ is also required for Dm8 survival or differentiation. Our findings suggest that Dpr-DIP interactions are important determinants of synaptic connectivity.

Keywords

synaptogenesis; cell adhesion; MiMIC; GFP tagging; optic lobe; immunoglobulin

[¶]Correspondence: zinnk@caltech.edu, eozkan@uchicago.edu.

Author contributions

R.A.C. analyzed *dpr* and *DIP* expression and phenotypes in larvae. K.P.M. analyzed expression and phenotypes in the OL. E.Ö. and M.E.B. performed the structural studies. S. N-J. and P-T. L. generated tagged MiMIC lines. M.J., E.Ö., and K.Z. generated the new Dpr-ome. K.Z., E.Ö., K.C.G., and H.B. analyzed data and supervised experiments.

Introduction

Neurons in the *Drosophila* brain make genetically specified synaptic connections within a dense neuropil in which neuronal processes come into contact with many possible targets, implying that, as proposed by Sperry, target neurons "must carry some kind of individual identification tags". His statement that "the growing fibers are extremely particular when it comes to establishing synaptic connections, each fiber linking only with certain neurons to which it becomes selectively attached by specific chemical affinities" (Sperry, 1963) applies well to compact hard-wired networks such as the fly brain.

The "labeled pathways hypothesis" proposed that each insect central nervous system (CNS) neuron expresses specific cell surface proteins (CSPs), called "surface labels", that function as identification tags or "Sperry molecules". Each of these proteins would be expressed on a small subset of neuronal growth cones, while its binding partner would mark the surfaces of neurons with which these growth cones interact. This binding partner might itself be a surface label for a different subset of neurons. It was also speculated that some surface labels might be found to be members of gene families (Goodman et al., 1984). While the labeled pathways hypothesis was developed primarily to explain axon guidance, these concepts can also be applied to synaptic specificity.

The *Drosophila* genome encodes ~1000 CSPs, representing more than 80 domain types, that are likely to participate in cell-cell recognition events (Kurusu et al., 2008), but there was no obvious way to identify potential surface labels among these. Unexpected insights emerged from an *in vitro* extracellular "interactome" (ECIA) screen of all *Drosophila* CSPs containing immunoglobulin superfamily (IgSF) and leucine-rich repeat (LRR) domains, in which all possible pairwise combinations were tested for binding. The most striking finding from these studies was that a subfamily of 2-Ig domain CSPs, the Dprs (Defective proboscis extension response proteins; (Nakamura et al., 2002)), selectively interacts with a 3-Ig domain CSP subfamily, which we denoted as DIPs (Dpr-interacting proteins). Dprs and DIPs form a complex interaction network, the "Dpr-ome", in which most Dprs bind to multiple DIPs and *vice versa* (Özkan et al., 2013).

As documented in this paper, the complete Dpr-ome contains 21 Dprs and 9 DIPs. *dpr1* is the only one of these 30 genes that has been previously characterized. *dpr1* mutants have reduced aversion to salt and exhibit courtship defects, and a *dpr1* reporter is expressed in subsets of brain neurons (Goldman and Arbeitman, 2007; Nakamura et al., 2002).

Here we describe the crystal structure of a Dpr-DIP complex, and show that 6 *dpr* and *DIP* genes are expressed by subsets of larval and pupal CNS neurons. Interactions between Dpr11 and its partner DIP-γ regulate larval neuromuscular junction (NMJ) development. In the pupal visual system, Dpr11 and DIP-γ are required for normal formation of synapses between photoreceptors and amacrine neurons. These results are consistent with the hypothesis that Dprs and DIPs are neuronal surface labels involved in the establishment of synaptic specificity during development.

Results

An updated and more complete version of the Dpr-ome

We discovered the Dpr-ome using the ECIA, a high-throughput, avidity-driven assay for interactions between extracellular proteins (Özkan et al., 2013). The published Dpr-ome contained several proteins ("orphans") with no binding partners. Since Dprs 4, 15, and 18 had expressed poorly, we created chimeras for those Dprs in which their first (D1) Ig domains were inserted in place of the D1 of Dpr6, a strong expressor. We also included a new Dpr we identified, Dpr21. We expressed the XCDs of all Dprs, Dpr chimeras, and DIPs as secreted Fc and pentamerized alkaline phosphatase (AP_5) fusion proteins and used them in an ECIA to create a more complete Dpr-ome (Figures 1A, S1C-D).

The revised Dpr-ome defines DIP binding partners for all Dprs except Dpr18. Interestingly, Dpr18 has nonconservative substitutions at three completely conserved sites within the D1 interface region (Figure S2A), suggesting that it may not be able to bind DIPs. However, *dpr18* is unlikely to be a pseudogene, because these changes are found in Dpr18 orthologs in other dipteran genomes. The Dpr-ome now contains 21 Dprs and 9 DIPs. Each Dpr interacts with 1-4 DIPs, and each DIP with 1-7 Dprs. The "common DIP" (cDIP), a secreted LRR protein of unknown function, binds to 14 Dprs and 7 DIPs (Figures 1A, S1C-D).

The molecular basis of DPR–DIP interactions

Dprs and DIPs interact in a defined pattern, creating a code that may impart specificity to interactions between cells expressing these proteins. To understand this code, it is necessary to define the molecular details of the interactions between Dprs and DIPs. The D1s of Dpr6 and DIP-α can form a complex (Figure S1A). We determined the crystal structure of Dpr6-D1 bound to DIP-α-D1D2, using the multi-wavelength anomalous diffraction method (Figures 1B-C and Table S1). The D1s interact with each other using the *CC'C"FG* faces of the immunoglobulin fold. The complex is pseudo-symmetric, *i.e.* the two Ig-type D1s are related to each other via a two-fold symmetry axis. This nearly orthogonal D1-D1 heterodimer topology bears a striking resemblance to several other Ig-type D1-D1 complexes. These include the SYG-1-SYG-2 complex, which initiates formation of synapses, the JAML-CAR complex, a signaling complex of the immune system, and Nectin complexes (Figures 1D-E)(Dong et al., 2006; Özkan et al., 2014; Samanta et al., 2012; Verdino et al., 2010). The appearance of this interaction geometry in multiple adhesive IgSF protein complexes suggests that it may represent an evolutionarily optimized binding solution for formation of cell-cell synapses.

Residues at the center of symmetry for both the JAML-CAR and SYG-1-SYG-2 complexes have polar side chains and can make hydrogen bonds or salt bridges (Figure 1D). By contrast, the core of the Dpr6-DIP-α interaction interface is strongly hydrophobic in nature, with van der Waals contacts dominating the interface and a buried surface area of 1900 $Å^2$ (Figures 2A, C, D and S2C-D). It does not contain any salt bridges. There are 15 hydrogen bonds at the interface, but only three do not involve main chain atoms. Therefore, charge complementarity and polar interactions are not the basis of binding specificity among Dprs and DIPs. Rather, shape complementarity is more likely to explain DPR-DIP specificity.

The S_c parameter (Lawrence and Colman, 1993) is 0.75, indicating highly complementary surfaces.

We confirmed the crystallographically observed Dpr-DIP interface by mutating interface residues and measuring affinity using surface plasmon resonance (SPR). All mutations of the interface diminished or abolished binding, except for Dpr6 H114A. This mutation increased affinity by 10-fold, a result of much slower dissociation kinetics (Figures 2B and S2E).

Our Dpr6-DIP-α structure serves as a template for all Dpr-DIP complexes, because Dpr and DIP D1 domains are well conserved. The average sequence identities among Dpr D1s and DIP D1s are 45% and 53%, respectively (Figure S2A). Furthermore, the chemical nature of the Dpr and DIP surfaces involved in the interaction is preserved in all Dprs and DIPs, but the residues are conservatively variable to accommodate the variety of Dpr/DIP complexes that need to be formed. The Dpr6 interface residue with the highest impact on binding affinity, Dpr6 Y123 (Figure 2B), is restricted to the closely related set of amino acids of Y, F and H. Similarly, the DIP-α residue most critical for binding, Q125, is invariant. The two contacting residues at the two-fold center of the interface, Dpr6 I115 and DIP-α I83 (Figures 1D, 2A), are limited to I, L or V among all Dprs and DIPs. We confirmed that the same interfaces are used in the Dpr11-DIP-γ complex by mutating Dpr11 residues I159 and F167 (corresponding to Dpr6 I115 and Y123), and DIP-γ residue V88 (corresponding to DIP-α I83). As observed for the Dpr6-DIP-α pair, changing any of these residues to Alanine weakened or abolished binding (Figures 2B, S2F).

Finally, specific hydrophobic interface residues correlate with binding of Dprs to particular DIPs. For example, F123 and I124 are unique to the four Dprs (11, 15, 16, 17) that bind to DIP-γ (Figures 1A, S2A). To a lesser degree, the use of hydrophobic residues to modulate shape complementarity has been seen in other cross-reactive receptor-ligand systems, such as the interactions of cytokines with their shared receptors gp130 and γ_c (Wang et al., 2009).

Dprs and DIPs are expressed by subsets of larval CNS neurons

To evaluate the expression and phenotypes of Dprs and DIPs, we utilized *Minos*-mediated integration cassette (MiMIC) insertions (Venken et al., 2011). MiMICs contain a gene-trap cassette, which consists of a strong splice acceptor (SA), followed by STOP codons, an EGFP coding sequence with its own ATG, and a polyA sequence. Hence, 5' UTR insertions, and some coding intron insertions, function as EGFP reporters that are expressed in the pattern of the gene's mRNA (Figures S3A-B). Insertions in 5' UTR and constitutive coding introns are highly mutagenic when the SA is in the (+) orientation, generating lethal phenotypes for >90% of essential genes (Nagarkar-Jaiswal et al., 2015). Coding intron insertions also permit the integration of an artificial exon encoding EGFP (SA-EGFP-splice donor (SD)) into coding sequence. Most such tagged proteins (denoted as X-EGFP-X) display the proper expression pattern and subcellular localization (Nagarkar-Jaiswal et al., 2015; Venken et al., 2011).

We tagged endogenous Dprs and DIPs by inserting EGFP in frame into coding sequence. We also converted MiMICs into transcriptional activators (drivers), which express reporters

in the pattern of the gene into which they are inserted. Converting a (−) intron MiMIC to a driver in the (+) orientation generates a new loss-of-function (LOF) mutation. The application of MiMIC technology to Dprs and DIPs reveals its remarkable utility in allowing the rapid exploration of gene families. MiMICs exist for 25 of the 30 *dpr* and *DIP* genes. We have already tagged 16 of the proteins with EGFP (see http://flypush.imgen.bcm.tmc.edu/pscreen/rmce/), and also generated GAL4 and QF drivers.

Figures 3 and S3 show expression in the 3rd instar larval ventral nerve cord (VNC) of MiMIC reporters for *dpr11* and its partners *DIP-γ* and *DIP-β*, and for *DIP-α* and its partners *dpr6* and *dpr10* (see Figure 1A). These are visualized together with motor neuron or cholinergic interneuron driver/reporters. There is partial overlap between the pattern of cell bodies expressing each gene and the labeled motor neurons and interneurons, but the coexpressing neurons are different in each case (Figure 3). Each MiMIC reporter labels a very different pattern of axon tracts and dendrites (Figures S3C-H). We also show expression of the $dpr11^{MiMIC\ MI02231\ 5'>EGFP}$ reporter (henceforth denoted as $dpr11^{MiMIC}$) together with nuclear dsRed driven by GAL4s for its two binding partners: $DIP\text{-}\gamma^{MiMIC\ MI03222\rightarrow GAL4}$ (henceforth denoted as *DIP-γ-GAL4*)(Figure 3E), and $DIP\text{-}\beta^{MiMIC\ MI01971\rightarrow GAL4}$ (Figure S3E). In both cases, there are neurons that express both *dpr11* and the partner gene, but the patterns of coexpressing neurons are different. In summary, these data show that each of the 6 genes is expressed by a distinct subset of larval motor neurons and interneurons.

$dpr11^{MiMIC}$ and $DIP\text{-}\gamma^{MiMIC\ MI03222\ 5'>EGFP}$ (henceforth denoted as $DIP\text{-}\gamma^{MiMIC}$) GFP reporters are both expressed by motor neurons, but reporter levels vary between cells (Figure 3). Reporters driven by *DIP-γ-GAL4* and by a GAL4 driver derived from *dpr11* control sequences ($dpr11^{GMR95G12}$) label NMJ presynaptic terminals, including the muscle 4 NMJ (Figures 4A, C), as does Dpr11-EGFP-Dpr11, a reporter for endogenous Dpr11 protein localization. Dpr11-EGFP-Dpr11 also exhibits postsynaptic staining surrounding muscle 4 NMJ boutons (Figure 4B), indicating that Dpr11 protein is expressed by muscles. Muscle GFP puncta are observed in *DIP-γ-GAL4>GFP* animals (Figure 4C), and rescue experiments (see below) suggest that *DIP-γ* is also likely to be expressed at low levels in muscles.

Dpr11-DIP-γ interactions regulate morphogenesis of NMJ presynaptic terminals

To evaluate the functions of Dpr11 and DIP-γ in NMJ development, we examined 3rd instar larvae bearing mutations in these genes. We used insertions in 5' UTR introns that would be expected to eliminate or reduce protein expression. For *dpr11*, these were $dpr11^{MiMIC}$ and a *pBac(SAstopDsRed)* mutation (Schuldiner et al., 2008), $dpr11^{LL01039}$. These were used as homozygotes or placed over a deficiency (*Df*), *Df(3R)BSC193*. For *DIP-γ*, we used $DIP\text{-}\gamma^{MiMIC}$ over *Df(3R)Exel6210*. *dpr11* and *DIP-γ* mutants are adult-viable.

In both *dpr11* and *DIP-γ* mutants, we observed NMJ phenotypes characterized by the presence of supernumerary clustered small boutons known as satellites (Figures 4D-F, S4A). The number of satellite boutons at the muscle 4 NMJ was increased by 5-6 fold relative to *wt* and by ~3-fold relative to heterozygous animals (Figure 4G). A transheterozygote ($dpr11^{MiMIC}/DIP\text{-}\gamma^{MiMIC}$) lacking one *wt* copy of each gene had an equally strong

phenotype. This type of interaction between two genes has been observed for other ligand-receptor pairs, including Slit-Roundabout and Semaphorin-Plexin (Kidd et al., 1999; Winberg et al., 1998), and suggests that the encoded proteins function in the same pathway. Consistent with this model, a double mutant lacking both *wt* copies of each gene had a phenotype no stronger than that of the single mutants (Figure 4G). Given that Dpr11 and DIP-γ bind selectively to each other (Figure 1A), we interpret these findings as an indication that Dpr11-DIP-γ interactions are rate-limiting for control of satellite bouton formation.

To define the cells in which Dpr11 and DIP-γ function, we conducted rescue experiments by expressing UAS constructs encoding Dpr11 and DIP-γ in neurons or muscles in the corresponding mutant background. Surprisingly, we observed that expression driven by either a pan-neuronal driver (Elav-GAL4) or a muscle-specific driver (myosin heavy chain(MHC)-GeneSwitch in the presence of RU486)(Osterwalder et al., 2001) fully rescued the satellite bouton phenotype for both *dpr11* and *DIP-γ* (Figure 4G). These results are consistent with a model in which adhesion complexes can form between the neuron and the muscle in which Dpr11 is presynaptic and DIP-γ is postsynaptic, as well as *vice versa*, and that the two types of complexes have equivalent functions in regulating presynaptic terminal maturation. However, the data do not exclude the possibility that *cis* Dpr11-DIP-γ complexes can form on motor neurons and/or on muscles and that these have functions during NMJ development.

Satellites are likely to be immature boutons, and are often observed in mutants in which the retrograde BMP signaling pathway, which controls NMJ arbor growth, is hyperactivated. In this pathway, a muscle-derived BMP ligand interacts with neuronal BMP receptors (reviewed by (O'Connor-Giles and Ganetzky, 2008)). To evaluate this for *dpr11* and *DIP-γ*, we generated transheterozygotes with one mutant copy of these genes combined with one copy of a lethal mutation, Dad^{j1E4}, in *Daughters against dpp* (*Dad*). *Dad* encodes a negative regulator of BMP signaling (Tsuneizumi et al., 1997) and interacts with other BMP pathway components to regulate NMJ development (Menon et al., 2015; Nahm et al., 2013; Sweeney and Davis, 2002). We observed strong interactions, indicating that loss of Dpr11 or DIP-γ affects BMP signaling (Figure 4G).

We also examined interactions between *dpr11* and *DIP-γ* and an activated BMP receptor subunit, Tkv^{ACT}. One copy of neuronally expressed UAS-Tkv^{ACT} does not affect satellite bouton number on its own, but it can synergize with mutations in BMP regulators (O'Connor-Giles et al., 2008). We found that combining neuronal UAS-Tkv^{ACT} with one mutant copy of *dpr11* or *DIP-γ* generated satellite bouton phenotypes (Figure 4G), confirming that Dpr11 and DIP-γ regulate signaling through the BMP pathway. Finally, we examined phosphorylated Mothers against dpp protein (pMad), which is commonly used as a readout for BMP signaling intensity. In *dpr11* mutants, pMad levels at the NMJ are greatly increased relative to *wt* (Figures 4H-I), indicating that BMP signaling is hyperactivated.

Dpr11 and DIP-γ regulate spontaneous activity at the NMJ

To assess the electrophysiological consequences of the loss of each protein, we recorded miniature excitatory postsynaptic potential (mEPSPs) and EPSPs at 3rd instar NMJs. We observed matching electrophysiological phenotypes for *dpr11* and *DIP-γ* mutants in which

mEPSP amplitude and frequency were increased to similar extents (Figures 4J-L, S4D-E). However, there was no effect on evoked responses (EPSPs; Figures S4B-C). mEPSP amplitude changes are usually associated with postsynaptic effects, while mEPSP frequency alterations are associated with presynaptic changes. In summary, the NMJ data show that the loss of either Dpr11 or DIP-γ causes the same defects in presynaptic terminal maturation and neurotransmission.

dprs and *DIPs* are expressed by optic lobe neurons that project to specific medulla layers

To examine whether Dprs and DIPs are involved in determining synaptic connectivity patterns, we examined their expression and function in the pupal and adult visual system. The retina has ~800 ommatidia (Om), each containing 8 photoreceptors (PRs), R1-R8. R1-R6 are used for motion detection, while R7 and R8 mediate color vision. R7 and R8 project directly to the medulla (Me), while R1-R6 connect indirectly with the Me through lamina (La) neurons. The Me is a 10-layered neuropil divided into ~800 columns. There are at least 60 types of Me neurons (Fischbach and Dittrich, 1989; Morante and Desplan, 2008). Their cell bodies are outside the neuropil, and each neuron arborizes and forms synapses in a specific set of Me layers. Local neurons are restricted to the Me, while projection neurons arborize in Me layers and send axons to the lobula (Lo) and lobula plate (Lop), which are higher-order centers that integrate input from Me columns and connect to the central brain (Figure 5A).

During late pupal stages, the *dpr11*^{MiMIC} reporter labels R7 axons and growth cones (see below), M3, and proximal Me layers (Figure 5B), while the *DIP-γ*^{MiMIC} reporter for its binding partner labels M3, M6, M8, and M10 (Figure 5C). A driver/reporter for Dpr11's other binding partner, DIP-β, labels M3 and M7, but not M6 (Figure S5A). Similarly, reporters for *dpr6*, *dpr10*, and their partner *DIP-α* each label different but overlapping patterns of Me layers (Figures 5D-F). Because the *dpr6* reporter is a tagged protein (Dpr6-EGFP-Dpr6), these data show that Dpr6 localizes to the neuropil (Figure 5D). In summary, each of the 6 *dprs* and *DIPs* is selectively expressed by optic lobe (OL) neurons that form synapses in specific Me layers.

dpr11 and *DIP-γ* are expressed by synaptic partners in the medulla

There are two types of ommatidia in an adult fly, yellow (y; ~70%) and pale (p; ~30%), which are randomly distributed (Wernet et al., 2006). yR7s express a longer-wavelength UV-sensitive opsin, Rh4, while pR7s express a shorter-wavelength opsin, Rh3. About two-thirds of mid-pupal R7 growth cones express the *dpr11* reporter (Figure 6A), suggesting that *dpr11* is specific to yR7s. To confirm this, we examined pupal retinas and showed that *dpr11* is selectively expressed by R7s in the pupal retina that also express an *Rh4* driver/reporter (Figure 6B).

R7s project to the M6 layer of the Me and make synapses with a variety of neurons. Dm8 neurons, which arborize in M6 and cover 13-16 columns (Figure 5A), receive more R7 synapses than any other target. R7s also synapse on Tm5a and Tm5b projection neurons (Gao et al., 2008; Karuppudurai et al., 2014; Takemura et al., 2013). We showed that *DIP-γ* is expressed in Dm8s by combining the *DIP-γ*^{MiMIC} reporter with a Dm8-specific split-

GAL4 driver/reporter (Gao et al., 2008). The two reporters are colocalized in M6 (Figure 6C), and a subset of Dm8s expresses both (see below). *DIP-γ* is also expressed in a subset of the cells that express a Tm5a/b-specific split-GAL4 driver/reporter (Karuppudurai et al., 2014)(Figure S6B).

To examine single *DIP-γ*-expressing neurons, we performed a "FLP-out" analysis by crossing *DIP-γ-GAL4* to a *UAS-FRT-stop-FRT-mCD8-GFP* reporter and a heat-shock promoter-driven FLP source (*hs-FLP*) and applying heat shocks during development to excise the stop sequence and label single neurons with GFP. We compared labeled neurons to neuronal profiles in (Fischbach and Dittrich, 1989) and (Takemura et al., 2013). We identified many Dm8s, which have a characteristic arborization pattern in M6, spanning multiple columns (Figure 6D). We also identified TmY9 and Mi4 (Figures S6C-D, 5A).

dpr11 and *DIP-γ* expression in synaptically connected neurons in the lobula plate

DIP-γ-GAL4 labels three lobula plate tangential cells (LPTCs), which are large neurons involved in motion detection (Figures S6E-F). There are three LPTCs in the horizontal system (HSN, HSE, HSS), 5-7 in the vertical system (VS), and two M cells. The distinctive dendritic morphology of the *DIP-γ-GAL4* FLP-out-labeled neuron in Figure 6E indicates that it is an HSN neuron (compare to Figure 20 of (Fischbach and Dittrich, 1989; Scott et al., 2002)).

dpr11 is expressed in subsets of both T4 and T5 cells (Figures 6F-H), which synapse on LPTCs. T4s and T5s are direction-selective neurons that respond to moving edges, and each has an axon that arborizes in one of the four layers of the Lop. Presentation of stimuli moving in a particular direction to flies expressing a genetically encoded Ca^{2+} indicator in T4s and/or T5s activates only those T4s/T5s specific for that direction and thus produces a signal in one Lop layer (Maisak et al., 2013). Remarkably, the *dpr11* reporter selectively labels Lop layers 1 (front-to-back) and 2 (back-to-front) (Figure 6F). The *DIP-γ*^{MiMIC} labels a zone encompassing Lop1 and Lop2 (Figure 6I), suggesting that the dendrites of the LPTCs that express *DIP-γ* are localized to the same layers to which the axons of *dpr11*-expressing neurons project. In summary, these data are consistent with a model in which Dpr11 is expressed on subsets of T4 and T5 neurons that signal motion along the fly's body axis and are presynaptic to LPTCs that express its binding partner DIP-γ.

Dpr11 and DIP-γ are required for normal connectivity between yR7s and Dm8s

To examine whether Dpr11-DIP-γ interactions are important determinants of synaptic connectivity in the visual system, we focused on synapses between Dpr11-expressing yR7s and DIP-γ-expressing Dm8s, which are their primary synaptic targets. To visualize yR7 terminals, we used the active zone reporter line *Rh4-LexA ::p65, 8XLexAop2-Brp-short*^{mCherry} (*Rh4>Brp-short*^{mCherry})(Berger-Muller et al., 2013). Bruchpilot (Brp) is an obligate active zone component at most or all synapses, and Brp-short^{mCherry} is a truncated form of Brp that labels existing active zones by associating with full-length Brp but cannot create new active zones when overexpressed (Berger-Muller et al., 2013; Fouquet et al., 2009). In adults heterozygous for *dpr11*^{MiMIC} or *DIP-γ*^{MiMIC}, yR7 terminals labeled by Brp-short^{mCherry} were bulb-shaped and regularly arranged in M6 (Figures 7A, C). A small

fraction of terminals (7-9%) in these controls had nub-like “overshoots” that extended deeper into M6 (Figures 7C, E).

In *dpr11*^{MiMIC}*/Df* adults, the percent of yR7 terminals displaying overshoots was greatly increased (**30.0**+/−1.8%, $p<0.0001$ relative to *dpr11*^{MiMIC}/+). A similar phenotype was observed in *DIP-γ*^{MiMIC}*/Df* (**19.2**+/−2.3%, $p=0.001$ relative to *DIP-γ*^{MiMIC}/+)(Figures 7B, D, E). These overshoots are qualitatively different from those in heterozygotes, with many extending through M6 and into the M7 layer. Also, the main bodies of most yR7 terminals in either mutant had irregular shapes and were not lined up at a fixed position along the vertical axis (Figures 7B, D). To more clearly visualize the morphologies of yR7 terminals, we generated surface renderings from high-magnification images using the Imaris program. We found that *dpr11* mutant terminals have irregular and extended shapes that protrude into M7 (Figures 7F-G). In summary, these data indicate that Dpr11 and DIP-γ are required for normal projection of yR7 terminals in the M6 layer.

To determine when the yR7 terminal phenotype becomes detectable, we labeled R7 growth cones at earlier stages of development. We observed no differences in yR7 growth cone morphologies between *dpr11/+* and *dpr11/Df* at 25 hr. (Figures 7H-I, S7E-F) and 50 hr. after puparium formation (APF)(Figures S7G-H). However, at 70 hr. APF, by which time R7 growth cones had begun to form presynaptic terminals in M6, we could see overshoot and terminal shape phenotypes in *dpr11/Df* animals (Figures S7I-J). These data suggest that loss of Dpr11 alters presynaptic terminal development but does not affect growth cone guidance.

The fact that the overshoot and terminal shape phenotypes are observed when either Dpr11 (expressed in yR7s) or DIP-γ (expressed in Dm8s) is absent suggests that these phenotypes arise from defects in yR7-Dm8 interactions mediated by Dpr11 and DIP-γ. However, only about 1/3 of Dm8s express *DIP-γ* (see below). Does this mean that *DIP-γ*$^{+}$ Dm8s are specific for yR7s? We obtained insights into this question by examining the relationships between yR7 terminals and the small gaps between *DIP-γ*$^{+}$ Dm8 arborizations in M6 that are observed in *DIP-γ*^{MiMIC}/+ animals (Figure 7C). Only 1 of 1042 yR7 terminals examined in 12 OLs was found in a gap. This suggests that yR7s may selectively target *DIP-γ*$^{+}$ Dm8s.

DIP-γ is required for survival or differentiation of Dm8 neurons

DIP-γ mutants had an additional phenotype that was not seen in *dpr11* mutants (Figures 7J-M, S7K). In single confocal slices from *DIP-γ*^{MiMIC}/+ adults, the M6 layer labeled by the GFP marker was almost continuous, while in *DIP-γ*^{MiMIC}*/Df* animals, there were large gaps in the M6 layer (Figures 7J-K). These were also seen when Dm8 arborizations were visualized in *DIP-γ* mutants using *Ort*^{C2b}*-GAL4>myristylated Tomato* (Figures 7L-M), but not when all neurons were labeled using anti-Brp (data not shown). Arborizations of single FLP-out-labeled Dm8s in *DIP-γ* mutants had a normal appearance (data not shown).

To define the origins of the M6 gap phenotype, we counted cells expressing the Dm8-specific *Ort*^{C2b}*-GAL4* driver that were positive or negative for the *DIP-γ*^{MiMIC} reporter. 34% of *Ort*$^{C2b+}$ Dm8s expressed *DIP-γ* in heterozygote controls (*DIP-γ*^{MiMIC}/+). The total number of Dm8s was decreased in *DIP-γ/Df* mutant adults as compared to these controls

(**352**+/−11 in controls, *vs.* **228**+/−5 in mutants, $p<0.0001$). Most of this decrease was due to the loss of Ort^{C2b+}, *DIP-*γ^{+} cells, whose numbers were decreased from **121**+/−5 in controls to **35**+/−2 in mutants ($p<.0001$)(Figures 7N-O, S7M-N). These data suggest that most Ort^{C2b+}, *DIP-*γ^{+} cells die or turn off the Ort^{C2b}*-GAL4* reporter when DIP-γ is not expressed.

Discussion

We have defined a network of interacting *Drosophila* IgSF CSPs in which 21 Dpr proteins bind to 9 DIPs. The structure of the Dpr-DIP complex resembles that of neural and immune cell adhesion complexes (Figures 1B-E). Each of the 6 *dpr* and *DIP* genes examined here is expressed by a different subset of neurons in the larval VNC and pupal OL (Figures 3, S3, 5, S5). In the larval neuromuscular system, Dpr11 and its binding partner DIP-γ regulate presynaptic terminal development and neurotransmission (Figures 4, S4). In the pupal OL, they are required for normal formation of synapses between a Dpr11-expressing sensory neuron and a DIP-γ expressing interneuron (Figures 6, 7, S7).

Implications of the Dpr-DIP complex structure

Our crystal structure (Figures 1B-E) shows that Dprs and DIPs belong to a group of IgSF CSPs that interact *via* their N-terminal Ig domains. These include immune cell receptors such as CD2, CD58, JAML, CAR, B7-1, and CTLA-4, and Nectin/Nectin-like (Necl) proteins. The 9 Nectin/Necls interact with each other, forming a small network (Dong et al., 2006; Samanta et al., 2012)(Figure 1E). Although DIPs resemble Nectins/Necls, their closest vertebrate counterpart is the 5-member IgLON subfamily, which is also expressed in neurons. Dprs have no clear mammalian orthologs. DIPs and Dprs are distinguished from IgLONs and Nectins in that their interactions are across subfamilies, not within a subfamily. The closest structural homolog of the Dpr-DIP complex is the SYG-1-SYG-2 complex, known to be involved in synapse specification (Özkan et al., 2014)(Figures 1D-E).

The Dpr-DIP complex has an interface involving no charge pairs, suggesting that binding specificity is encoded through shape complementarity (Figures 2C-D). The Dpr-DIP interaction code may be created by substitution of larger or smaller residues within the binding interface in order to create more or less complementary surfaces between individual interacting Dpr-DIP pairs. This differs substantially from the electrostatic complementarity model, in which receptor-ligand specificity is created primarily through hydrogen bonding interactions and salt bridges. Interestingly, for Dscam homophilic interactions, where each of the many thousands of possible variants binds primarily to itself, both electrostatic and shape complementarity play crucial roles(Sawaya et al., 2008). Each Dscam variant has to find a single binding solution, which is a task that can be solved in many ways. By contrast, the complex cross-reactivity observed for Dpr-DIP interactions may impose restrictions on encoding of specificity that mandate the selection of shape complementarity as the primary mechanism.

Dpr11-DIP-γ interactions regulate NMJ presynaptic terminal development

The larval neuromuscular system is a genetic model system for glutamatergic synapses in mammals (for review see (Menon et al., 2013)). In mutants lacking either Dpr11 or DIP-γ, NMJs contain many small clustered boutons called satellites. The satellite bouton phenotypes are rescued by either pre- or postsynaptic expression of the proteins. mEPSP amplitude and frequency are increased to similar extents in *dpr11* and *DIP-γ* mutants (Figures 4, S4). These data, together with the fact that the two loci genetically interact, indicate that the two proteins have linked functions, and suggest that the phenotypes are due to loss of Dpr11-DIP-γ adhesion complexes.

BMPs are trophic factors for mammalian neurons, and retrograde BMP signaling controls NMJ arbor growth in *Drosophila*. Satellites are observed in mutants in which BMP signaling is upregulated (O'Connor-Giles and Ganetzky, 2008). Consistent with this, presynaptic pMad staining, which reports on the magnitude of the BMP signal, is increased in *dpr11* mutants, and *dpr11* and *DIP-γ* interact with genes encoding BMP signaling components (Figure 4).

Development of normal connectivity between yR7s and Dm8s requires Dpr11 and DIP-γ

Each *dpr* and *DIP* we have examined is expressed in a unique subset of neurons that project to specific layers in the OL neuropils (Figures 5, S5, 6, S6). Identifying these neurons can define relationships between *dpr/DIP* expression and synaptic connectivity, because detailed synaptic maps for units of the first two areas of the OL, the La and Me, have been created using electron microscopic reconstruction (Rivera-Alba et al., 2011; Takemura et al., 2013).

Axons of UV-sensitive R7 photoreceptors synapse in layer M6 of the Me onto Dm8, Tm5a, Tm5b, and other targets (Gao et al., 2008; Karuppudurai et al., 2014; Takemura et al., 2013) (Figure 5A). *dpr11* is selectively expressed by yR7s, which express Rh4 opsin and are in approximately 70% of ommatidia (Figure 6)(Wernet et al., 2006). Dpr11 is the first cell surface protein to be associated with a subclass of R7s. *DIP-γ* is expressed by Dm8s, which arborize in M6 and receive more R7 synapses than any other neurons (Figure 6).

To examine whether formation of synapses between yR7s and Dm8s involves interactions between Dpr11 and DIP-γ, we expressed a marker for existing active zones, Brp-short^{mCherry}, in yR7s (Berger-Muller et al., 2013; Fouquet et al., 2009). In control animals, yR7 terminals are bulb-shaped and regularly arranged in M6. In *dpr11* and *DIP-γ* mutants, the main bodies of yR7 terminals have altered shapes, and active zone and membrane markers are found in extensions projecting into deeper Me layers (overshoot phenotype; Figures 7 and S7). These data suggest that synapses between yR7 and its M6 targets do not form normally in the absence of Dpr11 or DIP-γ. Because most M6-projecting *DIP-γ*-positive cells seen in the FLP-out analysis are Dm8s, and because Dpr11's other partner, DIP-β, does not label M6 (Figure S5), we infer that the loss of Dpr11 or DIP-γ is likely to primarily affect yR7-Dm8 synapses in M6 (Figure S7D).

DIP-γ is likely to regulate survival of Dm8 amacrine neurons

In *DIP-γ* mutants, there are large gaps in M6 labeling by *DIP-γ* or Dm8 reporters. The number of Ort^{C2b+}, *DIP-γ*$^{+}$ cells is reduced by >3-fold, suggesting that most *DIP-γ*-expressing Dm8s die (Figures 7, S7). Alternatively, they might turn off expression of the Ort^{C2b}*-GAL4* driver, although this seems less likely. This effect on cell fate suggests that DIP-γ is required for reception of a neurotrophic signal. Since *dpr11* mutants have no *DIP-γ*^{MiMIC} M6 gaps (Figure S7), implying that they have normal numbers of Ort^{C2b+}, *DIP-γ*$^{+}$ cells, this signal might be communicated through Dprs 15, 16, and/or 17, the other Dprs that bind to DIP-γ (Figure 1A). Other OL neurons are also dependent on trophic factors for survival. R cell growth cones secrete the Jelly Belly (Jeb) ligand, which binds to its receptor Alk on L3 neurons, and L3s die in the absence of Jeb or Alk (Pecot et al., 2014). The functions of DIP-γ in mediating normal development of yR7-Dm8 connectivity, as assayed by displacement of the active zone marker in yR7s, may be distinct from its roles in Dm8 survival, because about half of the overshoots in *DIP-γ* mutants appear to grow through a Dm8 arbor labeled by the *DIP-γ* reporter (Figure 7D).

Dpr-DIP interactions and the assembly of synaptic circuits

dpr11 is expressed by subsets of direction-selective T4 and T5 neurons that arborize in the Lop layers activated by front-to-back and back-to-front motion (Maisak et al., 2013), and *DIP-γ* is expressed by three LPTCs, which receive synaptic input from T4s and T5s (Figures 6, S6). These data suggest that Dpr11 and DIP-γ expression patterns might have evolved to facilitate assembly of synaptic circuits for specific sensory responses: near-UV vision for yR7-Dm8 connections, and movement along the anterior-posterior axis for T4/T5 subset-LPTC connections. In a conceptually similar manner, a specific type of vertebrate amacrine neuron, VG3-AC, forms synapses on W3B retinal ganglion cells, which are specialized for detecting object motion. Both VG3-ACs and W3B-RGCs selectively express the IgSF protein Sidekick2 (Sdk2), and Sdk2-mediated homophilic adhesion is required for their connectivity (Krishnaswamy et al., 2015).

An accompanying paper on gene expression in La neurons (Tan et al., submitted) presents 10 instances in which a La neuron expressing a Dpr is synaptically connected to a Me neuron expressing a DIP to which that Dpr binds *in vitro*. In 9 of these, as well as in the two cases described here (yR7→Dm8 and T4/T5→LPTC), the Dpr is in the presynaptic neuron and the DIP in the postsynaptic neuron. Each *dpr* and *DIP* gene examined in the two papers is expressed in a different subset of OL neurons, each of which projects to a distinct set of neuropil layers, and neurons can express multiple Dprs or DIPs or a combination of the two (Figures 3, S3, S6; Tan et al., submitted). This means that there are hundreds of different synaptic matches in the OL that could potentially be programmed by the Dpr-ome network. Dprs and DIPs are also expressed by subsets of neurons in other areas of the larval and pupal brain (Figure S5 and unpublished results). These expression patterns, together with the phenotypic data presented here for one Dpr-DIP binding pair, suggest that Dpr-DIP interactions are likely to be important determinants of synaptic connectivity during brain development.

Experimental Procedures

Drosophila Genetics

"*wt*" controls were w^{1118} x *Canton S*. MiMIC lines and derivatives are from the Bellen lab, and most are in the Bloomington Stock Center (BDSC). EGFP-tagged protein lines and GAL4/QF drivers were derived as described by (Nagarkar-Jaiswal et al., 2015; Venken et al., 2011). Additional information on lines and constructs is in **Extended Experimental Procedures**.

Immunohistochemistry and electrophysiology

Antibodies used for staining are listed in **Extended Experimental Procedures.** Imaging was performed on a Zeiss LSM510 confocal microscope with a 40X objective. Adobe Photoshop was used for image processing. Larval dissections and antibody staining were done essentially as described by (Menon et al., 2009). Comparison of pMad levels was performed on confocal images captured with identical settings. For satellite bouton phenotypes, satellites were counted for at least 8 muscle 4 NMJs in at least 8 larvae (>64 NMJs per genotype). Electrophysiological analysis was done as described by (Carrillo et al., 2010). Only muscles with a resting membrane potential of <−60mV were analyzed.

Optic lobe dissections and staining were done using published protocols(Hsiao et al., 2012; Walther and Pichaud, 2006). FLP-outs were done as in (Gao et al., 2008). For Dm8 FLP-outs, heat-shocks were given on day 5 for 5 minutes at 37°C. Counting of yR7 terminals labeled with Brp-short^{cherry} was done on a confocal *z*-stack with 0.6 μm sections at zoom 2. *z*-slices for all other experiments were 1 μm at zoom 1. Experiments on adult OLs were done on <24 hr old adults, except for those in Figure 7L-M, which were 5 days old. The 3D surface rendering of R7 terminals was generated using Imaris software (Bitplane). Dm8 cell body populations were counted by outlining all the Dm8s using the (Ort>dsRed) channel in 1 μm slices of the Me cortex region of a confocal *z*-stack, then marking the Dm8s that were positive in the *DIP-γ* (GFP MiMIC) channel.

Structural and biochemical analysis

ECIA experiments and Fc/AP_5 protein expression were done as described by (Özkan et al., 2013). Methods for protein purification, crystallography, and SPR are described in **Extended Experimental Procedures.**

Supplementary Material

Refer to Web version on PubMed Central for supplementary material.

Acknowledgments

We thank Maximilien Courgeon, Claude Desplan, and Takashi Suzuki for advice on OL experiments, Takashi Suzuki for Rh4>Brp-short^{mCherry}, Chi-hon Lee for Dm8 and Tm5a/b GAL4 drivers, Elizabeth Gavis for UAS-CD4-tdTomato, and the BDSC for other lines. We thank Larry Zipursky and Liming Tan for discussions and communication of data before publication. We thank Alexander Borst and Namrata Bali for discussions, Elena Armand, Suzanne Fischer, Deepa Waghray, and Kelsey Carter for technical assistance, and Violana Nesterova for help with Figure 5A. This work was supported by NIH RO1 grant NS62821 and R37 grant NS28182 to K.Z., and by the HHMI (H.J.B. and K.C.G. labs). Stanford Synchrotron Radiation Lightsource beamlines 11-1 and 12-2 at

SLAC National Accelerator Lab are supported by the U.S. Department of Energy, Office of Science, Office of Basic Energy Sciences (DE-AC02-76SF00515). The SSRL Structural Molecular Biology Program is supported by the DOE Office of Biological and Environmental Research and by the NIH, NIGMS (including P41GM103393). The accession number for the atomic coordinates and structure factors of the crystal structure reported in this paper is PDB: 5EO9.

References

Berger-Muller S, Sugie A, Takahashi F, Tavosanis G, Hakeda-Suzuki S, Suzuki T. Assessing the role of cell-surface molecules in central synaptogenesis in the Drosophila visual system. PLoS One. 2013; 8:e83732. [PubMed: 24386266]

Carrillo RA, Olsen DP, Yoon KS, Keshishian H. Presynaptic activity and CaMKII modulate retrograde semaphorin signaling and synaptic refinement. Neuron. 2010; 68:32–44. [PubMed: 20920789]

Dong X, Xu F, Gong Y, Gao J, Lin P, Chen T, Peng Y, Qiang B, Yuan J, Peng X, et al. Crystal structure of the V domain of human Nectin-like molecule-1/Syncam3/Tsll1/Igsf4b, a neural tissue-specific immunoglobulin-like cell-cell adhesion molecule. J Biol Chem. 2006; 281:10610–10617. [PubMed: 16467305]

Fischbach KF, Dittrich APM. The optic lobe of Drosophila melanogaster. I. A Golgi analysis of wild-type structure. Cell and tissue research. 1989; 258:441–475.

Fouquet W, Owald D, Wichmann C, Mertel S, Depner H, Dyba M, Hallermann S, Kittel RJ, Eimer S, Sigrist SJ. Maturation of active zone assembly by Drosophila Bruchpilot. J Cell Biol. 2009; 186:129–145. [PubMed: 19596851]

Gao S, Takemura SY, Ting CY, Huang S, Lu Z, Luan H, Rister J, Thum AS, Yang M, Hong ST, et al. The neural substrate of spectral preference in Drosophila. Neuron. 2008; 60:328–342. [PubMed: 18957224]

Goldman TD, Arbeitman MN. Genomic and functional studies of Drosophila sex hierarchy regulated gene expression in adult head and nervous system tissues. PLoS Genet. 2007; 3:e216. [PubMed: 18039034]

Goodman CS, Bastiani MJ, Doe CQ, du Lac S, Helfand SL, Kuwada JY, Thomas JB. Cell recognition during neuronal development. Science. 1984; 225:1271–1279. [PubMed: 6474176]

Hsiao HY, Johnston RJ, Jukam D, Vasiliauskas D, Desplan C, Rister J. Dissection and immunohistochemistry of larval, pupal and adult Drosophila retinas. J Vis Exp. 2012:e4347. [PubMed: 23183823]

Karuppudurai T, Lin TY, Ting CY, Pursley R, Melnattur KV, Diao F, White BH, Macpherson LJ, Gallio M, Pohida T, et al. A Hard-Wired Glutamatergic Circuit Pools and Relays UV Signals to Mediate Spectral Preference in Drosophila. Neuron. 2014; 81:603–615. [PubMed: 24507194]

Kidd T, Bland KS, Goodman CS. Slit is the midline repellent for the robo receptor in Drosophila. Cell. 1999; 96:785–794. [PubMed: 10102267]

Krishnaswamy A, Yamagata M, Duan X, Hong YK, Sanes JR. Sidekick 2 directs formation of a retinal circuit that detects differential motion. Nature. 2015; 524:466–470. [PubMed: 26287463]

Kurusu M, Cording A, Taniguchi M, Menon K, Suzuki E, Zinn K. A screen of cell-surface molecules identifies leucine-rich repeat proteins as key mediators of synaptic target selection. Neuron. 2008; 59:972–985. [PubMed: 18817735]

Lawrence MC, Colman PM. Shape complementarity at protein/protein interfaces. J. Mol. Biol. 1993; 234:946–950. [PubMed: 8263940]

Maisak MS, Haag J, Ammer G, Serbe E, Meier M, Leonhardt A, Schilling T, Bahl A, Rubin GM, Nern A, et al. A directional tuning map of Drosophila elementary motion detectors. Nature. 2013; 500:212–216. [PubMed: 23925246]

Menon KP, Andrews S, Murthy M, Gavis ER, Zinn K. The translational repressors Nanos and Pumilio have divergent effects on presynaptic terminal growth and postsynaptic glutamate receptor subunit composition. J Neurosci. 2009; 29:5558–5572. [PubMed: 19403823]

Menon KP, Carrillo RA, Zinn K. Development and plasticity of the Drosophila larval neuromuscular junction. WIREs Developmental Biology. 201310.1002/wdev.108

Menon KP, Carrillo RA, Zinn K. The translational regulator Cup controls NMJ presynaptic terminal morphology. Molecular and cellular neurosciences. 2015; 67:126–136. [PubMed: 26102195]

Morante J, Desplan C. The color-vision circuit in the medulla of Drosophila. Curr Biol. 2008; 18:553–565. [PubMed: 18403201]

Nagarkar-Jaiswal S, Lee PT, Campbell ME, Chen K, Anguiano-Zarate S, Cantu Gutierrez M, Busby T, Lin WW, He Y, Schulze KL, et al. A library of MiMICs allows tagging of genes and reversible, spatial and temporal knockdown of proteins in Drosophila. eLife. 2015; 4

Nahm M, Lee MJ, Parkinson W, Lee M, Kim H, Kim YJ, Kim S, Cho YS, Min BM, Bae YC, et al. Spartin regulates synaptic growth and neuronal survival by inhibiting BMP-mediated microtubule stabilization. Neuron. 2013; 77:680–695. [PubMed: 23439121]

Nakamura M, Baldwin D, Hannaford S, Palka J, Montell C. Defective proboscis extension response (DPR), a member of the Ig superfamily required for the gustatory response to salt. J Neurosci. 2002; 22:3463–3472. [PubMed: 11978823]

O'Connor-Giles KM, Ganetzky B. Satellite signaling at synapses. Fly. 2008; 2:259–261. [PubMed: 20798607]

O'Connor-Giles KM, Ho LL, Ganetzky B. Nervous wreck interacts with thickveins and the endocytic machinery to attenuate retrograde BMP signaling during synaptic growth. Neuron. 2008; 58:507–518. [PubMed: 18498733]

Osterwalder T, Yoon KS, White BH, Keshishian H. A conditional tissue-specific transgene expression system using inducible GAL4. Proc Natl Acad Sci U S A. 2001; 98:12596–12601. [PubMed: 11675495]

Özkan E, Carrillo RA, Eastman CL, Weiszmann R, Waghray D, Johnson KG, Zinn K, Celniker SE, Garcia KC. An Extracellular Interactome of Immunoglobulin and LRR Proteins Reveals Receptor-Ligand Networks. Cell. 2013; 154:228–239. [PubMed: 23827685]

Özkan E, Chia PH, Wang RR, Goriatcheva N, Borek D, Otwinowski Z, Walz T, Shen K, Garcia KC. Extracellular architecture of the SYG-1/SYG-2 adhesion complex instructs synaptogenesis. Cell. 2014; 156:482–494. [PubMed: 24485456]

Pecot MY, Chen Y, Akin O, Chen Z, Tsui CY, Zipursky SL. Sequential axon-derived signals couple target survival and layer specificity in the Drosophila visual system. Neuron. 2014; 82:320–333. [PubMed: 24742459]

Rivera-Alba M, Vitaladevuni SN, Mishchenko Y, Lu Z, Takemura SY, Scheffer L, Meinertzhagen IA, Chklovskii DB, de Polavieja GG. Wiring economy and volume exclusion determine neuronal placement in the Drosophila brain. Curr Biol. 2011; 21:2000–2005. [PubMed: 22119527]

Samanta D, Ramagopal UA, Rubinstein R, Vigdorovich V, Nathenson SG, Almo SC. Structure of Nectin-2 reveals determinants of homophilic and heterophilic interactions that control cell-cell adhesion. Proc Natl Acad Sci U S A. 2012; 109:14836–14840. [PubMed: 22927415]

Sawaya MR, Wojtowicz WM, Andre I, Qian B, Wu W, Baker D, Eisenberg D, Zipursky SL. A double S shape provides the structural basis for the extraordinary binding specificity of Dscam isoforms. Cell. 2008; 134:1007–1018. [PubMed: 18805093]

Schuldiner O, Berdnik D, Levy JM, Wu JS, Luginbuhl D, Gontang AC, Luo L. piggyBac-based mosaic screen identifies a postmitotic function for cohesin in regulating developmental axon pruning. Dev Cell. 2008; 14:227–238. [PubMed: 18267091]

Scott EK, Raabe T, Luo L. Structure of the vertical and horizontal system neurons of the lobula plate in Drosophila. J Comp Neurol. 2002; 454:470–481. [PubMed: 12455010]

Sperry RW. Chemoaffinity in the Orderly Growth of Nerve Fiber Patterns and Connections. Proc Natl Acad Sci U S A. 1963; 50:703–710. [PubMed: 14077501]

Sweeney ST, Davis GW. Unrestricted synaptic growth in spinster-a late endosomal protein implicated in TGF-beta-mediated synaptic growth regulation. Neuron. 2002; 36:403–416. [PubMed: 12408844]

Takemura SY, Bharioke A, Lu Z, Nern A, Vitaladevuni S, Rivlin PK, Katz WT, Olbris DJ, Plaza SM, Winston P, et al. A visual motion detection circuit suggested by Drosophila connectomics. Nature. 2013; 500:175–181. [PubMed: 23925240]

Tsuneizumi K, Nakayama T, Kamoshida Y, Kornberg TB, Christian JL, Tabata T. Daughters against dpp modulates dpp organizing activity in Drosophila wing development. Nature. 1997; 389:627–631. [PubMed: 9335506]

Venken KJ, Schulze KL, Haelterman NA, Pan H, He Y, Evans-Holm M, Carlson JW, Levis RW, Spradling AC, Hoskins RA, et al. MiMIC: a highly versatile transposon insertion resource for engineering Drosophila melanogaster genes. Nat Methods. 2011; 8:737–U780. [PubMed: 21985007]

Verdino P, Witherden DA, Havran WL, Wilson IA. The molecular interaction of CAR and JAML recruits the central cell signal transducer PI3K. Science. 2010; 329:1210–1214. [PubMed: 20813955]

Walther RF, Pichaud F. Immunofluorescent staining and imaging of the pupal and adult Drosophila visual system. Nature protocols. 2006; 1:2635–2642. [PubMed: 17406519]

Wang X, Lupardus P, Laporte SL, Garcia KC. Structural biology of shared cytokine receptors. Annual review of immunology. 2009; 27:29–60.

Wernet MF, Mazzoni EO, Celik A, Duncan DM, Duncan I, Desplan C. Stochastic spineless expression creates the retinal mosaic for colour vision. Nature. 2006; 440:174–180. [PubMed: 16525464]

Winberg ML, Noordermeer JN, Tamagnone L, Comoglio PM, Spriggs MK, Tessier-Lavigne M, Goodman CS. Plexin A is a neuronal semaphorin receptor that controls axon guidance. Cell. 1998; 95:903–916. [PubMed: 9875845]

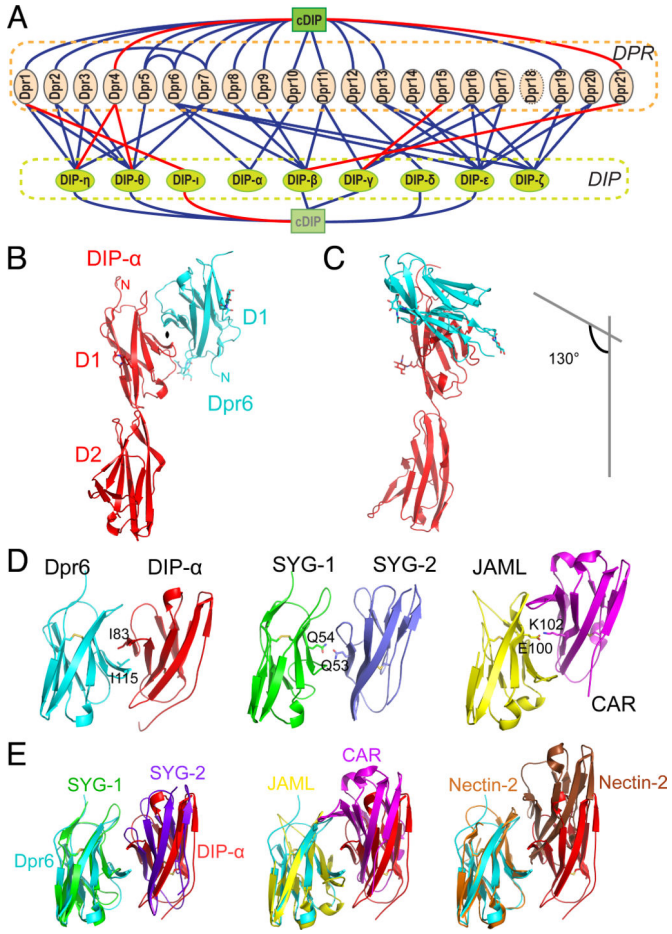

Figure 1. The Dpr-ome network and the structure of the Dpr-DIP complex

(A) The current Dpr-ome. New interactions identified in this study are in red.

(B) Structure of Dpr6-D1D2 bound to DIP-α-D1. The complex is formed by interactions between the D1s only. The D1s are related to each other by a near-symmetrical two-fold axis (closed oval). N-linked sugars are shown as sticks.

(C) The same structure rotated to show the 130° angle between the interacting domains and the angle of approach of the two proteins.

(D) Comparison of the DPR-DIP complex structure with two similar IgSF CAM complexes. Side chains for residues at the centers of interface are shown as sticks.

(E) Superimposition of the Dpr6-DIP-α complex onto related D1 complexes. Dpr6 is in cyan and DIP-α in red. Note that the overall path of the main chains is almost identical to those in the SYG-1-SYG-2 complex. The Dpr6-DIP-α complex is less similar to JAML-CAR, and diverges most from the homophilic Nectin-2 complex.

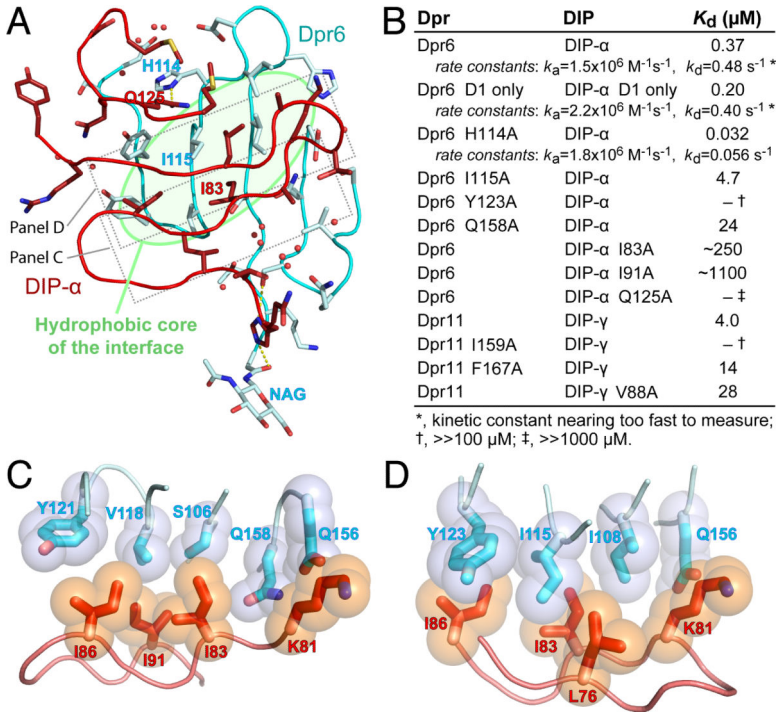

Dpr	DIP	K_d (μM)
Dpr6	DIP-α	0.37
rate constants: k_a=1.5x10^6 M^{-1}s^{-1}, k_d=0.48 s^{-1} *		
Dpr6 D1 only	DIP-α D1 only	0.20
rate constants: k_a=2.2x10^6 M^{-1}s^{-1}, k_d=0.40 s^{-1} *		
Dpr6 H114A	DIP-α	0.032
rate constants: k_a=1.8x10^6 M^{-1}s^{-1}, k_d=0.056 s^{-1}		
Dpr6 I115A	DIP-α	4.7
Dpr6 Y123A	DIP-α	– †
Dpr6 Q158A	DIP-α	24
Dpr6	DIP-α I83A	~250
Dpr6	DIP-α I91A	~1100
Dpr6	DIP-α Q125A	– ‡
Dpr11	DIP-γ	4.0
Dpr11 I159A	DIP-γ	– †
Dpr11 F167A	DIP-γ	14
Dpr11	DIP-γ V88A	28

*, kinetic constant nearing too fast to measure; †, >>100 μM; ‡, >>1000 μM.

Figure 2. Shape complementarity in the Dpr-DIP interface

(A) The interaction interface between Dpr6 (cyan) and DIP-α (red) is strongly hydrophobic and contains no salt bridges. The three side chain-to-side chain hydrogen bonds, including Dpr6 H114-DIP-α Q125, are labeled as dashes. The hydrophobic residues at the center of the interface, Dpr6 I115 and DIP-α I83, are also labeled. NAG represents the N-acetyl-DGlucosamine glycan residue on Dpr6 D1.

(B) Equilibrium and kinetic parameters measured for the interactions between wild-type and mutant versions of Dpr6 and DIP-α, and Dpr11 and DIP-γ using SPR. For several mutants, binding kinetics were too fast to measure. Raw binding curves are in Figures S2E-F.

(C) and (D) Rows of Dpr6 and DIP-α residues interdigitate, leading to shape complementarity between the two surfaces. Interestingly, Dpr6 Q156/158 and DIP-α K81 sidechains, while packing closely, do not form hydrogen bonds.

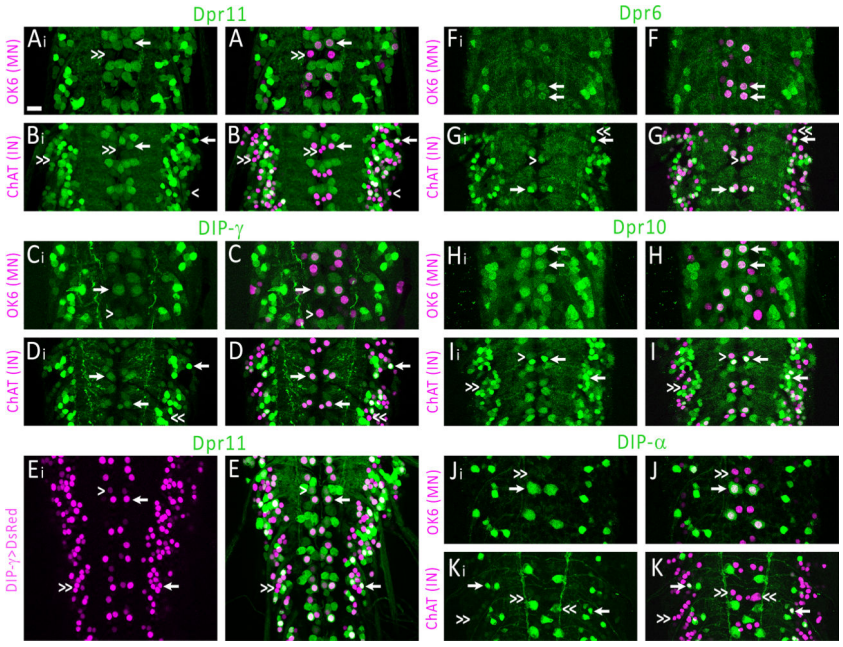

Figure 3. Expression of *dpr* and *DIP* genes in the larval ventral nerve cord

Projections of 3-6 confocal slices showing EGFP expression (green) and GAL4-driven nuclear dsRed expression (magenta) from: $dpr11^{MiMIC\ MI02231\ 5'>EGFP}$ (A, B, E), $DIP\text{-}\gamma^{MiMIC\ MI03222\ 5'>EGFP}$ (C, D), $dpr6^{MiMIC\ MI04582\ GT}$ (F, G), $dpr10^{MiMIC\ MI03557\ GT}$ (H, I), and $DIP\text{-}\alpha^{MiMIC\ MI02031\ GT}$ (J, K). GT=gene trap. GAL4 drivers were: OK6 (motor neurons) (A, C, F, H, J); ChAT (cholinergic interneurons)(B, D, G, I, K); or $DIP\text{-}\gamma^{MiMIC\ MI03222 \rightarrow GAL4}$ (E). Arrows: cells expressing both dsRed reporter and GFP at high levels. Carets: cells expressing dsRed and low levels of GFP. Double carets: cells that express only dsRed. Caret in (E): a cell that has GFP but only low levels of dsRed. Focal planes are different for OK6 and ChAT images, so different *dpr/DIP* cells are seen. One pair of $OK6^{+}$ dorsal midline motor neurons expresses *dpr11* and *DIP-γ*, the other pair expresses *DIP-α* at high levels and *DIP-γ* at low levels, and *dpr6* and *dpr10* are expressed by both pairs. Scale bar: 5 μm.

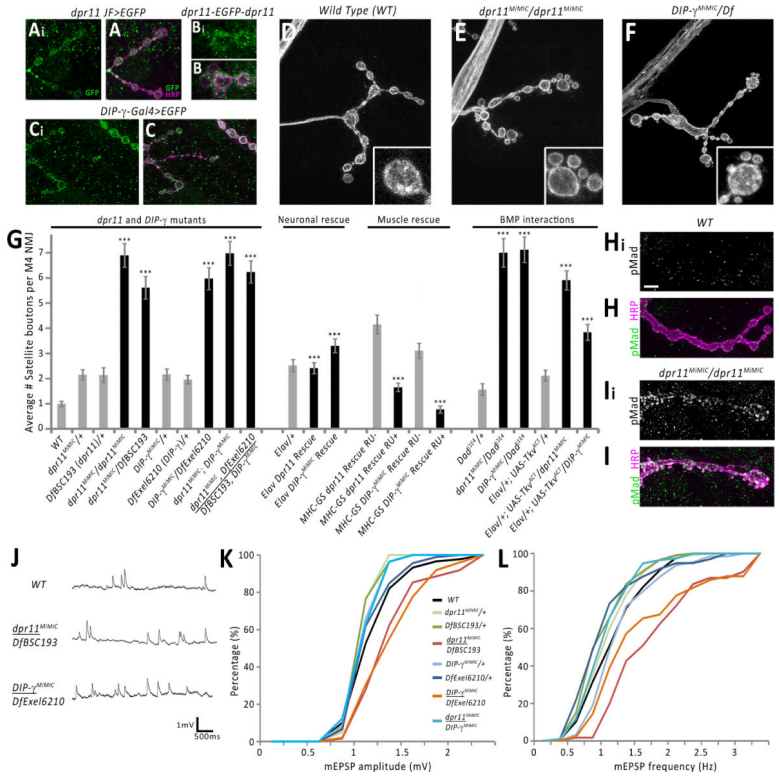

Figure 4. *dpr11* and *DIP-γ* NMJ phenotypes

Panels A-I are muscle 4 NMJs.

(A, Ai) GFP driven by *dpr11*^{GMR95G12}-GAL4 (Janelia Farm) labels boutons (arrows). Note green puncta on the muscle surface. Magenta: anti-HRP. Scale bar: 5 μm.

(B, Bi) Dpr11-EGFP-Dpr11 outlines anti-HRP-labeled boutons, and is observed postsynaptically outside of bouton borders (arrowhead) and on the muscle surface. Scale bar: 2 μm.

(C, Ci): EGFP driven by *DIP-γ*$^{MiMIC\ MI03222\rightarrow GAL4}$ labels boutons (arrow). Note green puncta on the muscle surface. Scale bar: 5 μm.

(D-F) *dpr11* and *DIP-γ* mutants have satellite bouton phenotypes (arrows indicate satellites). Anti-HRP staining. Insets: single 1b boutons. Scale bar: 5 μm.

(G): Quantitation of satellite bouton phenotypes. Experimental genotypes in black, controls in grey. $p<.0001$ (***) for differences between relevant genotypes.

(H-I): pMad is elevated at the NMJ in *dpr11* mutants. Scale bar: 5μm.

(J): Tracings of spontaneous events. Recordings from muscles 6 and 7.

(K-L): Cumulative probability graphs of mEPSP amplitude (J) and mEPSP frequency (K). The curves for *dpr11* and *DIP-γ* mutants (red and orange) are shifted to the right relative to all other genotypes. $p<.0001$ for mEPSP frequency change relative to controls, $p<.001$ for mEPSP amplitude (see Figure S4).

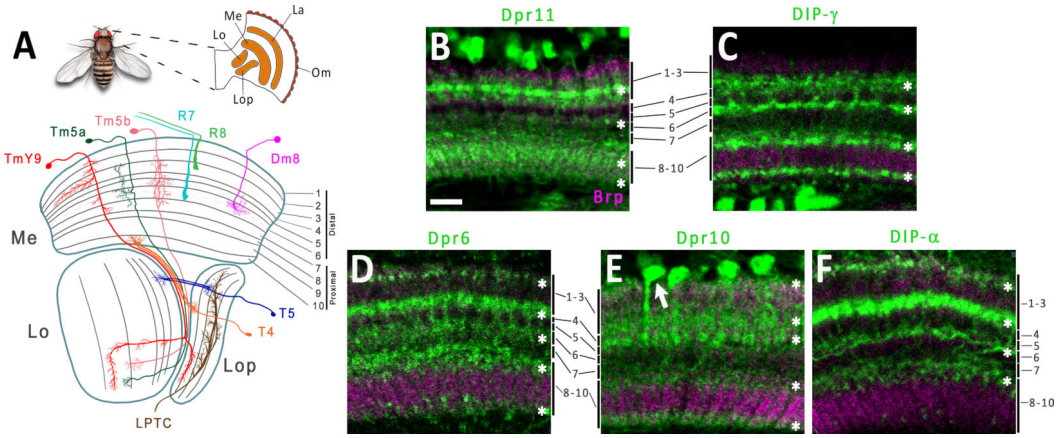

Figure 5. *dprs* and *DIPs* are expressed in optic lobe neurons projecting to specific medulla layers

(A) The Me, Lo, and Lop areas of the OL. Top images show OL orientation relative to the fly head. Me neuropil layers are labeled and profiles of neurons of interest are superimposed onto the diagram. Adapted from (Fischbach and Dittrich, 1989).

Panels B-F are projections of 3-4 confocal slices of 80 hr. APF medullas. nc82 (anti-Brp; magenta) was used to identify neuropil layers (marked on the sides of panels). Asterisks highlight labeled layers; layer numbers are indicated at the sides of the panels.

(B) *dpr11*$^{MiMIC\ MI02231\ 5'>EGFP}$ labels M3, M6 (weak) and M8-10.

(C) *DIP-γ*$^{MiMIC\ MI03222\ 5'>EGFP}$ labels M3, M6, M8, and M10.

(D) Dpr6-EGFP-Dpr6 labels M1, M4, M6, M8, and M10.

(E) *dpr10*$^{MiMIC\ MI03557\ GT}$ labels M1, M3, M4, M8 (weak) and M10.

(F) *DIP-α*$^{MiMIC\ MI02031\ GT}$ labels M1, M3, M6, and M8.

Scale bar: 10 μm for all panels.

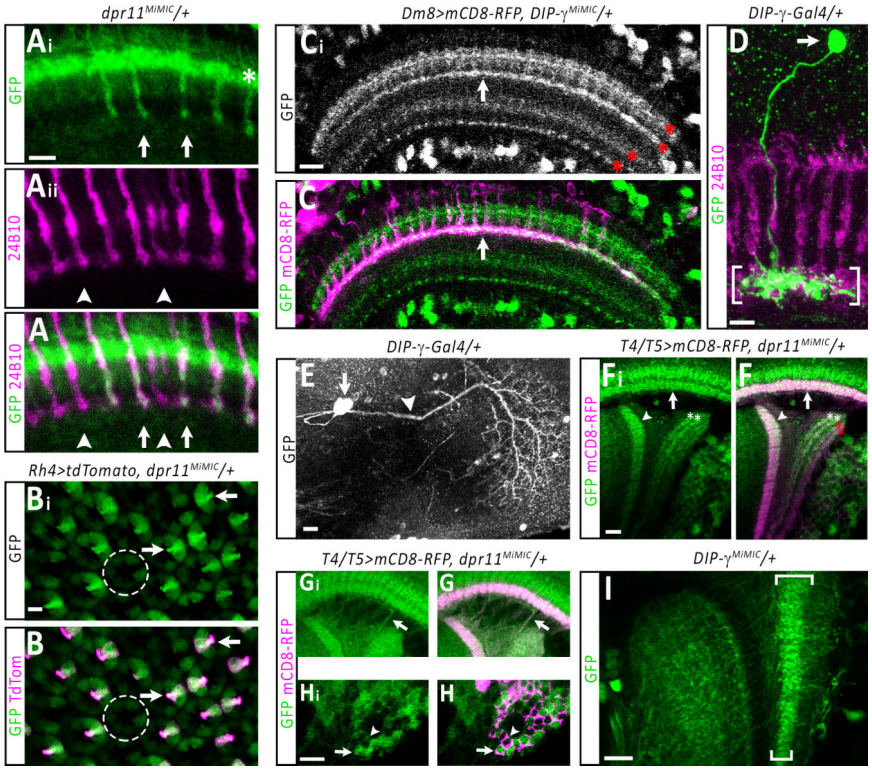

Figure 6. *dpr11* and *DIP-γ* are expressed by synaptically connected neurons

(A) R7 growth cones in M6 at 47 hr. APF, labeled by *dpr11*$^{MiMIC\ MI02231\ 5'>EGFP}$ (green) and 24B10 (magenta). A subset of R7s (arrows) express *dpr11*. Arrowheads, pR7s express only 24B10. Green layer is M3 (asterisk). Scale bars for (A-B): 5 μm.

(B) *dpr11*$^{MiMIC\ MI02231\ 5'>EGFP}$ is selectively expressed by Rh4>tdTomato-expressing yR7s (magenta; arrows) in pupal retina at 80 hr. APF. Dotted circles outline a p (Rh3) ommatidium.

(C) *DIP-γ*$^{MiMIC\ MI03222\ 5'>EGFP}$ (white/green) labels M6 (arrows) at 47 hr. APF and colocalizes with a mCD8-RFP reporter driven by a Dm8-specific split-GAL4 driver (magenta). Red asterisks, *DIP-γ* expressing Me layers. Scale bar: 10 μm.

(D) FLP-out labeling of a single *DIP-γ*$^{MiMIC\ MI03222\rightarrow GAL4}$ expressing Dm8 (green), in an adult. R7/R8 axons are labeled by 24B10 (magenta). Brackets, M6 arborization; arrow, cell body. Scale bar: 5 μm.

(E) FLP-out labeling of a single *DIP-γ*$^{MiMIC\ MI03222\rightarrow GAL4}$ expressing LPTC, in an adult. Cell body, arrow; main dendrite, arrowhead.

(F) *dpr11* is expressed by T4 and T5 cells, as shown by double labeling with *dpr11*$^{MiMIC\ MI02231\ 5'>EGFP}$ (green) and a T4/T5-specific GAL4, R42F06, driving mCD8-RFP (magenta). Arrow, T4 dendrites in M10; arrowhead, T5 dendrites in Lo1. Note that, although there are 4 layers of the Lop labeled by the driver (magenta/white in panel F; asterisks), only Lop1 and Lop2 have green GFP labeling in panel Fi (white asterisks).

(G) M10 labeling by *dpr11*$^{MiMIC\ MI02231\ 5'>EGFP}$ reflects *dpr11* expression by T4s, because T4 axons connecting M10 to the Lop are double-labeled (arrows).

(H) A subset of T4 and T5 cell bodies are labeled by *dpr11*$^{MiMIC\ MI02231\ 5'>EGFP}$. A T4 /T5 cell bodies that expresses *dpr11* (arrow) and one that does not (arrowhead) are labeled.

(I) *DIP-γ*$^{MiMIC\ MI03222\ 5'>EGFP}$ labels a zone in the Lop spanning Lop1/2 (brackets) at 47 hr. APF, most likely representing LPTC dendrites. Scale bars for (E-H): 10 μm.

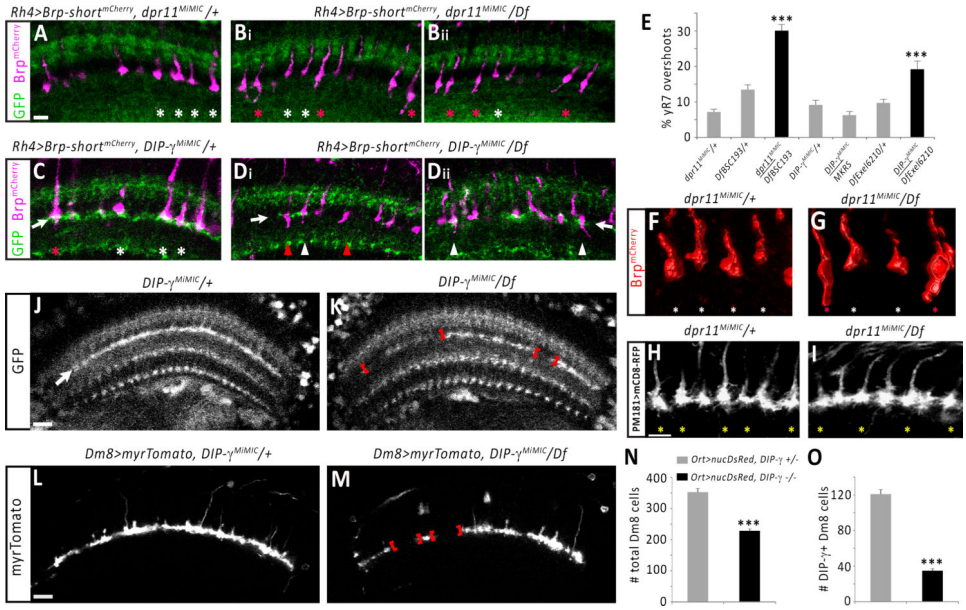

Figure 7. *dpr11* and *DIP-γ* mutations affect yR7 terminals and Dm8 cell numbers

(A) In *dpr11*^{MiMIC}/+ adults, Brp-short^{mCherry} labeled yR7 terminals (magenta; white asterisks) line up in M6 at a point defined by the dark/light demarcation line in the EGFP labeling (green). Scale bar for (A-D): 5 μm.

(B) In *dpr11*^{MiMIC}*/Df* adults, some yR7s overshoot M6 and grow into deeper layers (red asterisks). White asterisks: yR7s that do not overshoot. Note that the shapes of all terminals are irregular, and that they are not aligned along the vertical axis.

(C) In *DIP-γ*^{MiMIC}/+ adults, Brp-short^{mCherry} labeled yR7 terminals (magenta; white asterisks) are superimposed on Dm8 arborizations (green; arrow) labeled by EGFP. Red asterisk: a yR7 scored as an overshoot.

(D) In *DIP-γ*^{MiMIC}*/Df* adults, some yR7s overshoot and terminal shape and alignment are altered, as in *dpr11* mutants. Red triangles indicate yR7 overshoots in gaps where no *DIP-γ*$^{+}$ Dm8 is present, and white triangles highlight yR7 overshoots that grow through a *DIP-γ*$^{+}$ Dm8 arbor (arrows).

(E) Quantitation of overshoot phenotypes. Overshoots tend to extend further in mutants (B, D) than in controls (C), but we have scored mutant and control overshoots as the same phenotype because we lack a quantitative way to distinguish them.

(F-G) Imaris surface renderings of yR7 terminals in *dpr11*^{MiMIC}/+ (F) and *dpr11*^{MiMIC}*/Df* (G). White asterisks, terminals at normal positions; red asterisks, overshoot terminals.

(H-I) R7 growth cones at 25 hr. APF in *dpr11*^{MiMIC}/+ (H) and *dpr11*^{MiMIC}*/Df* (I), visualized using PM181-GAL4 driving tdTomato. Asterisks indicate yR7s, identified by the *dpr11*^{MiMIC} GFP marker.

(J,K) In single confocal slices from *DIP-γ*^{MiMIC}/+ adults, the GFP-labeled M6 layer is continuous, but it has large gaps (red brackets) in *DIP-γ*^{MiMIC}*/Df*.

(L,M) M6 gaps (brackets) are also seen in *DIP-γ* mutants when Dm8 arborizations are labeled using a Dm8-specific split-GAL4 driver/reporter. Scale bars for (F-I): 10 μm.

(N,O) Quantitation of numbers of Ort^{C2b+} Dm8s (N) and of Ort^{C2b+} *DIP-*γ^{+} Dm8s (O) per OL in *DIP-*γ^{MiMIC}/+ and *DIP-*γ^{MiMIC}*/Df*.